

RESEARCH PAPER Open Access

Abnormal wind speed detection and prediction: methodology and case study



Yuting Yang^{1*}, Cong Zhang², Kin-Man Lam², Xin Sun³ and Yu Xue⁴

Abstract

Accurate wind speed prediction is crucial for conserving power resources and enhancing power utilization efficiency. However, deviations from typical wind patterns can introduce errors into predictions, potentially leading to imbalances between wind power supply and demand. Consequently, developing a model to forecast abnormal wind speeds is essential. To address this, we leverage the microcanonical multifractal formalism algorithm to detect abnormal wind speeds. In this paper, we integrate ensemble empirical mode decomposition, phase space reconstruction, and long short-term memory (LSTM) networks to predict these anomalies. Initially, wind speed data is meticulously pre-processed to generate datasets for one-hour, one-day, and non-zero wind speeds. Subsequently, LSTM networks are used to forecast abnormal wind speeds. Evaluations of our methodology across different datasets demonstrate its effectiveness, particularly excelling in one-hour forecasts.

Keywords Long short-term memory, Phase space reconstruction, Ensemble empirical mode decomposition, Time series, Dynamic analysis

1 Introduction

Wind energy utilization has become increasingly popular owing to its environmental benefits, global applicability, and cost-effectiveness (Nelson 2009; Bórawski et al. 2020). Wind power generation systems are crucial for harnessing wind energy and converting it into usable power, with their capacity influenced by weather conditions and generator states (Che et al. 2016; Liu et al. 2016). The relationship between wind energy and wind power is inherently nonlinear, often represented by a cubic function of wind speed. Recent studies have developed more sophisticated algorithms to elucidate

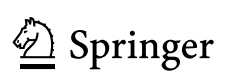
the conversion process between wind energy and wind power (Lei et al. 2018). Accurate wind power forecasting is vital for wind power systems as precise forecasts enable timely decision-making, reducing operational and resource costs (Lange and Focken 2006; Choi et al. 2009; Li et al. 2013).

Wind speed serves as the fundamental input for wind power forecasting, with predictions spanning various time scales: medium (weekly), long-term (monthly), short-term (daily), and ultra short-term (hourly). Medium- and long-term forecasts primarily inform instrument maintenance planning, wind farm planning, and annual generation planning. However, the accuracy and reliability of short-term predictions are crucial for mitigating wind curtailment and optimizing power generation plans (Neshat et al. 2020; Kamath and Senapati 2021). Furthermore, ultra short-term predictions provide essential information for optimizing frequency regulation, managing reserve capacity, and real-time wind power optimization and scheduling (Wang and Yang 2021).

Yuting Yang

yangyuting@stu.ouc.edu.cn

⁴ College of Engineering, Ocean University of China, Qingdao 266100,



^{*}Correspondence:

College of Computer Science and Engineering, Shandong University of Science and Technology, Qingdao 266590, China

² Department of Electrical and Electronic Engineering, The Hong Kong Polytechnic University, Hong Kong 999077, China

³ Faculty of Data Science, City University of Macau, Macao 999078, China

Given the intermittent nature of wind speed fluctuations caused by sudden changes and potential generator failures, there is a critical need to ensure the safe and efficient operation of wind power systems. This paper proposes using the LSTM model (Hochreiter and Schmidhuber 1997) for predicting abnormal wind speeds, leveraging historical wind speed data. Renowned for its effectiveness in addressing regression problems, LSTM demonstrates promise in handling inherent sequential regularities within wind speed time-series data (Lin et al. 2020; Shahid et al. 2021; Li and Yang 2023). Recent studies have further validated the efficacy of LSTM's efficacy in wind speed forecasting. For instance, Demirtop and Sevli (2024) proposed a hybrid model combining LSTM with the ARIMA approach to enhance forecasting accuracy, leveraging LSTM's capability to capture long-term dependencies while ARIMA addresses linear patterns. Additionally, Leme Beu and Landulfo (2024) applied LSTM networks to estimate wind speed profiles over complex terrains, demonstrating superior performance over traditional methods, such as the power law, particularly at higher altitudes. This indicates LSTM's potential in modeling intricate wind patterns. Moreover, Mohapatra et al. (2023) proposed a hybrid approach integrating ARIMA, Kalman filter, and LSTM to effectively capture both linear and nonlinear patterns in wind speed data, resulting in improved prediction accuracy. Nonetheless, LSTM's susceptibility to local minima remains a challenge. To address this, we propose a hybrid approach that combines time-series-based and spatial correlation-based methods with LSTM to enhance prediction accuracy. The proposed methodologies are detailed in the following section. Experimental results and corresponding analyses are presented in Section 3, followed by a comprehensive summary of the contributions of this paper in Section 4.

2 The proposed method

This paper addresses the challenge of accurately predicting abnormal wind speeds by proposing a novel approach that integrates ensemble empirical mode decomposition (EEMD) (Wu and Huang 2009), phase space reconstruction (Packard et al. 2008), and LSTM networks. The proposed prediction model encompasses several key steps, commencing with data pre-processing to prepare the wind speed data for different prediction tasks. EEMD is then employed to mitigate noise by decomposing the time-series data into simpler components. This step is crucial for managing the inherent complexity of wind speed data. Following this, we determine the optimal embedding dimension and delay time to reconstruct the time series, further refining the data by minimizing noise. The LSTM model is then applied to forecast wind speeds based on the processed data. Lastly, we employ rigorous evaluation methods to assess the model performance of the proposed methodology. By integrating these techniques, we aim to enhance the accuracy and reliability of abnormal wind speed predictions, thereby contributing to the optimization and efficiency of wind power systems.

2.1 Data pre-processing

Utilizing wind speed data gathered every 10 min over a year, we have constructed three distinct datasets to predict abnormal wind speeds: the one-hour, one-day, and non-zero wind speed datasets. This strategic segmentation is crucial for capturing the diverse temporal patterns in wind behavior, as abnormal wind speed events can occur over varying time scales. By structuring our datasets in this manner, we aim to identify subtle patterns and fluctuations in wind behavior across different time intervals. This meticulous dataset enables us to account for the diverse temporal characteristics of abnormal wind speed events, facilitating the development of robust predictive models tailored to specific forecasting horizons. Consequently, our approach enhances the accuracy and adaptability of abnormal wind speed predictions, thereby boosting the efficacy and reliability of wind power systems.

The one-hour wind speed dataset is constructed based on wind speed data sampled every 10 min. By extracting readings at six intervals, we create a dataset that captures wind speed dynamics over one-hour periods, as illustrated in Fig. 1b. This segmentation allows for analyzing fine-grained variations in wind speed dynamics over hourly wind variations.

By contrast, the non-zero wind speed dataset is introduced for comparative analysis. Zero entries are replaced to maintain consistency, and similar to the one-hour dataset, readings are sampled at six-point intervals to form one-hour segments. Subsequently, for the non-zero wind speed dataset, we sample wind speed readings at six-point intervals to create one-hour segments. This dataset allows for comparative assessments of wind speed behaviors under varying conditions, thereby enriching our understanding of wind dynamics and improving predictive models. This meticulous dataset design supports robust analyses and fosters advancements in wind power forecasting methodologies.

The one-day wind speed dataset, depicted in Fig. 1c, is devised to provide insights into wind speed patterns over extended time intervals. Starting with data collected at six-point intervals to form the one-hour dataset, we aggregate 24 consecutive data points to create a comprehensive view of wind speed dynamics over a 24-hour period. By delineating wind speed variations across daily time scales, this dataset offers valuable insights into the long-term behavior and trends of wind

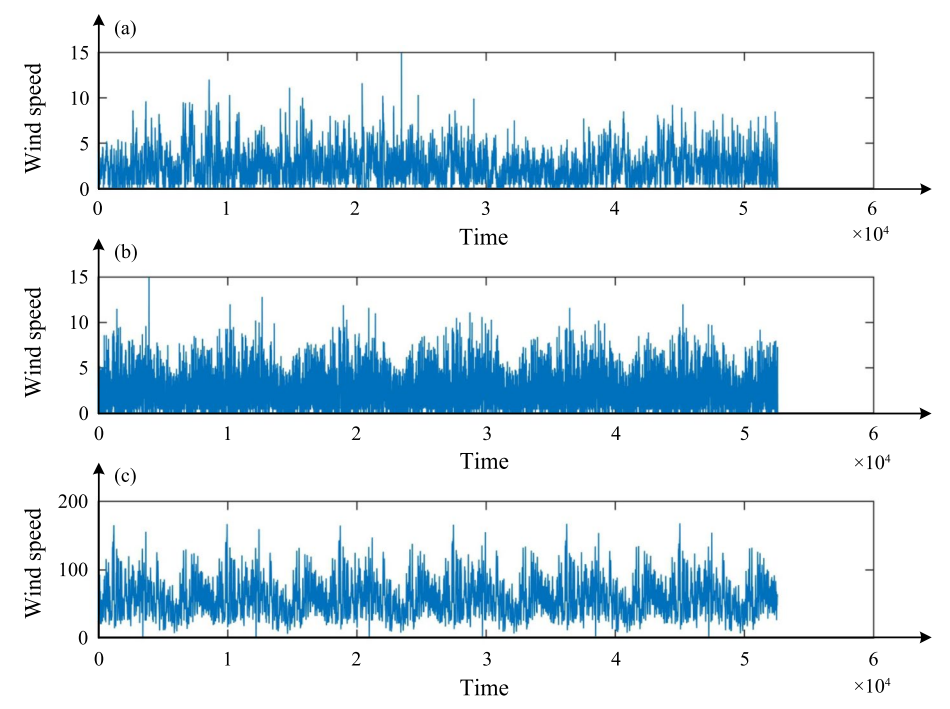


Fig. 1 Wind speed time series used in this paper. **a** Wind speed data collected every 10 min. **b** Sampled every 6 points from the wind speed data **a**. **c** Summation of every 24 adjacent points from **b**

patterns. Such insights are crucial for informing strategic decisions related to energy planning, resource allocation, and operational scheduling within wind power systems. It also supports comprehensive analyses and model validations, thereby enhancing the accuracy and reliability of wind speed forecasting methodologies.

We also employ the MMF to detect abnormal wind speeds (García-Marín et al. 2013). MMF, renowned for its efficacy in identifying irregular structures and chaotic systems, presents a robust framework for discerning anomalous wind speed behaviors (Suman and Hussein 2019). By analyzing variations between adjacent points within wind speed time-series data, MMF facilitates the detection of singular exponents (SEs). SE values quantify the magnitude of variations in the wind speed time-series, with higher SE fractions greater heightened variability. In our methodology, we designate the top 20% of SE values as indicative of abnormal wind speeds. By implementing MMF-based detection techniques, we enhance the ability of our predictive models to identify and anticipate anomalous wind speed events accurately. Consequently, this approach refines wind power forecasting methodologies, leading to more informed decision-making and improved operational efficiency in wind power systems. This step prepares the data for subsequent phase space reconstruction.

2.2 EEMD

Empirical mode decomposition (EMD) is well-suited for arbitrary data as it decomposes signals based solely on their inherent characteristics without relying on predefined basis functions. EMD operates under the assumption that signals comprise intrinsic mode functions (IMFs) with both linear and nonlinear traits. This assumption allows EMD to extract a series of IMFs from the input signal, each capturing specific temporal and frequency components, providing a comprehensive representation of the signal's underlying dynamics. This adaptive nature of EMD enables it to effectively capture and isolate the varying modes of an input signal, regardless of its complexity or structure. This makes EMD a versatile and powerful tool for signal decomposition and analysis across a wide range of applications and data types.

EEMD (Wu and Huang 2009) enhances the conventional EMD algorithm (Wu and Huang 2004) by offering improved noise reduction capabilities. Unlike EMD, which decomposes the input signal into IMFs (Chang et al. 2009) using a single deterministic process, EEMD conducts multiple tests. Each test applies EMD to a duplicate of the input signal with added noise. While individual tests may yield noisy results, the aggregated IMF components from multiple tests facilitate noise cancellation as the added white noise is evenly distributed

across the time-frequency space. By employing a filter bank, the time-frequency space is decomposed into IMF components of varying frequencies. Averaging these results cancels out noise, leaving a pure signal decomposition. Importantly, as the number of tests conducted increases, additional noise is progressively eliminated, preserving only the persistent signal component. This iterative process enables EEMD to effectively suppress noise while maintaining the integrity of the underlying signal, thereby improving the reliability and accuracy of subsequent wind speed predictions. A series of IMFs can be obtained by decomposing the signal using the EEMD method as follows:

$$x(t) = \sum_{i=1}^{n-1} IMF_i(t) + r(t),$$
(1)

where $IMF_i(t)$ is the *i*-th IMF obtained by EEMD decomposition at t time step. The component r(t), often denoting the trend of the signal, represents the residual after decomposing n-1 IMFs. The number of IMF terms is determined by the signal itself, with decomposition continuing until the residual meets specified criteria. In our experimental setup, the wind speed time series undergoes EEMD decomposition, resulting in 15 distinct terms. The first 14 terms represent the IMFs, arranged in descending order of frequency, while the final term corresponds to the residual component, encapsulating the information not captured by the preceding IMFs. This decomposition scheme enables a comprehensive analysis of the wind speed time series, facilitating the identification and characterization of its underlying temporal and frequency components with enhanced granularity and fidelity. EEMD effectively addresses noise issues inherent in wind speed time-series data, providing a foundation for reliable predictions.

2.3 Phase space reconstruction

Phase space reconstruction is crucial for analyzing chaotic time-series data, which can be viewed as a sequence of observations evolving over time. To extract meaningful insights from such data, Packard et al. (2008) introduced two methods for phase space reconstruction: the derivative reconstruction method and the coordinate delay reconstruction method. The coordinate delay reconstruction technique represents the underlying dynamics of the time series in a higher-dimensional space, revealing patterns and structures not apparent in the original one-dimensional data. By leveraging phase space reconstruction, analysts can gain deeper insights into the underlying dynamics of chaotic systems and improve the accuracy of subsequent analyses and predictions. This reconstruction

technique involves constructing a d dimensional phase space vector y(t) from a one-dimensional timeseries x(t), utilizing a specified delay time τ . This technique can be operationalized by using the subsequent formula:

$$y(t) = (x(t), \dots, x(t + (d-1)\tau)),$$
 (2)

where $1 \le t \le n - (d-1)\tau$. This phase space reconstruction technique relies on two crucial parameters: the embedded dimension d and the delay time τ . Embedding theory suggests optimal values for these parameters; however, specific expressions are not provided. In practice, time-series data are finite sequences often noisy, requiring a careful determination of suitable values for the embedding dimension and delay time based on the characteristics of the specific time series. In this study, we employ the mutual information (MI) method to compute the optimal time delay and utilize the falsenearest method (FNN) algorithm to ascertain the appropriate embedding dimension (Wallot and Mønster 2018). By leveraging these techniques, we ensure that the phase space reconstruction accurately captures the underlying dynamics of the time-series data, thereby enhancing the robustness and reliability of subsequent analyses and predictions.

In probability theory and information theory, MI serves as a pivotal metric that quantifies the degree of interdependence between two random variables. To determine the optimal time delay for multiple embedded time series, the average mutual information (AMI) method is employed, allowing the visualization of MI across multiple time series. Conceived by Wallot and Mønster (2018), AMI offers insights into how one random variable informs us about another. In time-series analysis, AMI is crucial for quantifying the information gained about $x(t+\tau)$ when observing x(t). By leveraging AMI, analysts can better understand the relationships between variables in time-series data, thereby enhancing the accuracy and reliability of analyses and predictions. In this paper, we define,

$$I(S,Q) = (x(t), x(t+\tau)),$$
 (3)

where $1 \le t \le n - \tau$, S represents the value of x at time t, and Q denotes the value of x at time $t + \tau$. Then, I(S, Q) is a function of the delay time τ , which can be written as $I(\tau)$. $I(\tau) = 0$ indicates that x(t) and $x(t + \tau)$ are completely unrelated. The first minimum of $I(\tau)$ shows that x(t) and $x(t + \tau)$ have the highest probability of being uncorrelated, which is also the optimal delay time τ .

From a geometric perspective, a chaotic time-series can be seen as the projection of the intricate trajectory of chaotic motion in a high-dimensional phase space onto a simpler one-dimensional space. This projection degrades the original trajectory of chaotic motion, causing non-adjacent points in the high-dimensional phase space to appear adjacent in the one-dimensional space.

Phase space reconstruction aims to restore the original trajectory from the observed chaotic time-series. As the embedding dimension increases, the structure of the chaotic motion orbit is clarified, reducing fault adjacent points. Consequently, the entire trajectory of chaotic motion can be more accurately recovered. This fundamental concept is central to the FNN algorithm.

In this study, we employ the FNN algorithm, initially proposed by Wallot and Mønster (2018), to determine the optimal embedding dimension (Kennel et al. 1992). The method operates on the principle that truly adjacent points in the original phase space should remain nearest neighbors even after embedding. If their distance significantly changes, they are deemed false-nearest neighbors, indicating an insufficient embedding dimension d. Consequently, the embedding dimension d is iteratively augmented until the number of false-nearest neighbors is sufficiently minimized.

Our implementation entails gradually increasing the embedding dimension d until the proportion of falsenearest neighbor points falls below 5% or their count stops decreasing. This iterative approach ensures that the embedding dimension d is appropriately determined, facilitating a more accurate representation of the underlying dynamics within the chaotic time-series data.

2.4 MMF

For calculating the singular exponents (SEs), we utilize an innovative framework called the MMF. This formalism leverages the magnitude of fluctuations observed among neighboring pixels within sea surface temperature (SST) images. By assessing these fluctuations relative to the scale of oceanographic features, such as fronts and eddies, MMF facilitates their efficient detection. A key aspect of MMF lies in the accurate determination of SE values.

A technique delineated in Pont et al. (2013) offers a robust approach for numerically computing SE values $h(\vec{x})$ at each pixel. This method is founded on the wavelet projection of the measure, ensuring computational stability. By employing this approach, we achieve a reliable assessment of SE across the SST images, thereby enhancing our ability to accurately discern and characterize oceanographic phenomena. The computational formula employed in this methodology is articulated as follows:

$$h(\overrightarrow{x}) = \frac{\frac{\log(\tau_{\psi}\mu(\overrightarrow{x}, r_0))}{<\tau_{\psi}\mu(., r_0)>}}{\log r_0} + o(\frac{1}{\log r_0}). \tag{4}$$

The scale r_0 is used for image normalization, given an image with size $N \times M$ corresponds to size 1 so that $r_0 = \frac{1}{N \times M}$. $\tau_{\psi} \mu(., r_0)$ is chosen as the average value of the wavelet projection over the entire signal. Accordingly, $\tau_{\psi} \mu(x, r_0)$ corresponds to the wavelet projection at point x. A fraction of the smallest SE values, also known as the most singular manifold (MSM), indicates the highest strength of variations among pixels in the SST image. Furthermore, owing to intermittency and multiscale organization, the MSM is composed of the most unpredictable points, characterized by the least values of SE. The MSM is defined as follows:

$$F_{\infty} = \overrightarrow{x} : h(\overrightarrow{x}) = h_{\infty} = \min(h(\overrightarrow{x})).$$
 (5)

2.5 The long-short-term memory

The LSTM network represents a specialized variant of recurrent neural networks engineered specifically to address long-term dependency challenges. Initially proposed by Hochreiter and Schmidhuber (1997), with subsequent enhancements by Alex Graves (Shi et al. 2021; Tao et al. 2021; Chi et al. 2022), LSTM has garnered widespread adoption across various domains. Central to LSTM is the cell state, which serves as its core functionality.

LSTM architecture comprises four distinct gates: the forget gate, input gate, output gate, and update gate. These gates enable LSTM to selectively retain or discard information within the cell state through a meticulously crafted structure referred to as a 'gate'. Each gate operates as a conduit for information, incorporating a functional layer and point-wise multiplication.

The use of sigmoid and hyperbolic tangent (tanh) functions is fundamental to LSTM's gate mechanisms. Specifically, sigmoid functions are typically applied to the forget, input, and output gates, whereas tanh functions are employed with the update gate. These functions yield outputs ranging from 0 to 1, delineating the degree to which each component contributes to information passage through the gate structure, thus providing LSTM networks with adaptive learning capabilities. These functions are defined as follows:

$$C^t = g^f \cdot C^{t-1} + g^i \cdot g, \tag{6}$$

$$h^t = g^o \cdot \tanh(C^t), \tag{7}$$

where g^f , g^i , g^o , g are the forget, input, output, and update gates, and C^{t-1} and C^t represent the previous and

current cell states, respectively. h^t denotes the current hidden state.

In the LSTM architecture, the input time-series data, alongside the previously stored cell state, are concurrently directed to the input gate g^i , forget gate g^f , and update gate g. These gates function as selective filters, allowing only pertinent portions of the input information to traverse through. The retained information, along with the previous cell state C^{t-1} , is updated to yield the current cell state C^t . Using the output gate, the current cell state is utilized to compute the current hidden state h^t .

The computed hidden state, along with the current cell state, is passed to the subsequent LSTM cell. This mechanism enables the cyclical circulation of information within the LSTM network, allowing for partial retention and dissemination of information across iterations. Consequently, the LSTM framework orchestrates a dynamic interplay between input data and internal states, thereby facilitating effective information flow and retention throughout the network operation.

3 Experimental results and analysis

In this paper, we propose an integrated approach that combines EEMD, phase space reconstruction, and LSTM networks for predicting abnormal wind speeds. EEMD is employed to mitigate noise in the wind speed time-series data, thereby enhancing the signal-to-noise ratio. Concurrently, phase space reconstruction techniques distill essential information from the time-series data, providing a more insightful representation of the underlying dynamics.

LSTM networks are employed for wind speed prediction owing to their inherent capability to model sequential dependencies effectively. Notably, LSTM outperforms traditional linear methods and feed-forward networks in sequence prediction tasks, demonstrating its efficacy across diverse research domains. The LSTM model architecture is implemented using the Keras-LSTM package, with the mean absolute error as the loss function and the Adam optimization algorithm for model training.

The proposed approach is validated using a dataset comprising 35000 wind speed observations for model training and 10000 observations reserved for model testing. This rigorous methodology aims to provide insights into predicting abnormal wind speeds, offering potential applications in various fields such as renewable energy, weather forecasting, and environmental monitoring.

3.1 Experimental data

The wind speed dataset used in this study originates from the Huangxian wind tower situated in China recorded in 2017, where measurements were recorded at 10 min intervals, resulting in a comprehensive time series spanning 52560 data points. Measurements were taken from an array of anemometers at various heights: 10 m, 50 m, 80 m, 90 m, 100 m, 110 m, and two at 120 m. Consequently, this dataset comprises eight distinct wind speed time series, each covering a one-year period, forming the foundation for all experimental analyses conducted in this study.

Wind speed measurements are susceptible to fluctuations due to atmospheric dynamics such as air pressure differentials, precipitation, wind direction variability, and potential anemometer malfunctions, leading to aberrant data. These anomalies manifest in two primary forms: deviations identified using the MMF method and instances of zero wind speed readings.

In this paper, prediction efficacy is evaluated using two established metrics: RMSE and the F_Score . These analytical tools facilitate a rigorous assessment of predictive accuracy, offering insights into the robustness and reliability of the proposed forecasting methodologies.

3.2 Evaluation methods

RMSE is used to measure the performance of the wind speed prediction model and is expressed as follows:

$$RMSE = \sqrt{\frac{\sum_{n=1}^{i=1} (X_{\text{obs},i} - X_{\text{model},i})^2}{n}},$$
(8)

where $X_{\text{model},i}$ and $X_{\text{obs},i}$ represent the predicted wind speed and the expected wind speed, respectively.

Furthermore, *PRE*_{zero} and *PRE*_{ab} denote the prediction accuracy of abnormal and zero wind speeds, which are computed as follows:

$$PRE_{zero} = \frac{TP_{zero}}{TP_{zero} + FP_{zero}},$$
(9)

$$PRE_{ab} = \frac{TP_{ab}}{TP_{ab} + FP_{ab}},\tag{10}$$

where $TP_{\rm zero}$ and $TP_{\rm ab}$ indicate the counts of predicted wind speed samples identified as zero and abnormal when the true wind speed sample is indeed zero and abnormal. Conversely, $FP_{\rm zero}$ and $FP_{\rm ab}$ represent the counts of predicted wind speed samples classified as zero and abnormal, respectively, while the true wind speed sample is non-zero and not indicative of abnormal conditions.

 REC_{zero} and REC_{ab} represent the recall rate and are computed as follows:

$$REC_{zero} = \frac{TP_{zero}}{TP_{zero} + FN_{zero}},$$
(11)

$$REC_{ab} = \frac{TP_{ab}}{TP_{ab} + FN_{ab}}. (12)$$

In speed prediction, $TP_{\rm zero}$ and $TP_{\rm ab}$ denote the counts of predicted wind speed samples identified as zero and abnormal, respectively, when the actual wind speed sample is zero and abnormal. Conversely, $FN_{\rm zero}$ and $FN_{\rm ab}$ represent the counts of predicted wind speed samples classified as non-zero and not indicative of abnormal conditions, respectively, while the true wind speed sample is zero and abnormal.

F_Score is proposed to simultaneously evaluate the recall rate and correct prediction rate (Fourure et al. 2021), which is computed as follows:

$$F_{\rm zero} = 2 * \frac{REC_{\rm zero} * PRE_{\rm zero}}{REC_{\rm zero} + PRE_{\rm zero}},$$
(13)

$$F_{ab} = 2 * \frac{REC_{ab} * PRE_{ab}}{REC_{ab} + PRE_{ab}}, \tag{14}$$

where F_{zero} and F_{ab} are used to evaluate the prediction performance for zero and abnormal wind speeds, respectively.

In this paper, three sets of experiments are conducted to evaluate the performance of our proposed prediction model for one-hour, one-day, and non-zero wind speed predictions.

3.3 The performance evaluated on one-hour wind speed time-series

In this experiment, the LSTM network is used for one-hour wind speed prediction. As shown in Table 1, the prediction accuracy of zero wind speed F_{zero} is lower than 19.67%, and the prediction accuracy of abnormal wind speed F_{ab} is lower than 37.34%. In the table, pos_i , $i = 1, \dots, 6$, represents the anemometers at heights of

10 m, 50 m, …, 110 m, respectively. pos_7 and pos_8 represent the two anemometers at the height 120 m in two different directions. The results show that the LSTM network can hardly predict zero and abnormal wind speeds.

For comparison, we propose integrating EEMD, phase space reconstruction, and LSTM techniques to forecast one-hour abnormal wind speeds. Initially, the one-hour wind speed time series is decomposed using EEMD, followed by reconstruction with phase space reconstruction. Subsequently, the LSTM model is deployed for wind speed prediction. As delineated in Table 2, the RMSE values across all eight positions using the proposed methodology remain below 0.8878. Notably, while the RMSE for the proposed method on the one-hour dataset slightly exceeds that of the standalone LSTM model, it performs better in terms of F_{zero} and F_{ab} metrics. Specifically, the proposed method yields F_{zero} values surpassing 32.00% and $F_{\rm ab}$ values exceeding 59.85% across all eight positions, outperforming the LSTM approach. These findings suggest that our proposed methodology enhances the accuracy of ultra-short-term prediction for zero and abnormal wind speeds.

3.4 The performance evaluated on one-day wind speed time-series

As illustrated in Table 3, the *RMSE* values achieved by the proposed methodology on the one-day dataset consistently exceed 13.0654 across all eight positions, significantly higher than those obtained on the one-hour dataset. Furthermore, the $F_{\rm ab}$ metric computed on the one-day wind speed dataset falls below 53.15% across all positions, notably lower than its counterpart derived from the one-hour wind speed dataset. These outcomes collectively suggest that predicting abnormal wind speeds over a one-day period is more challenging than forecasting over a one-hour duration.

 Table 1
 Prediction performance on one-hour wind speed dataset using LSTM model

	pos_1	pos_2	pos_3	pos_4	pos_5	pos_6	pos_7	pos_8
RMSE	0.5633	0.6709	0.7703	0.8003	0.7964	0.8317	0.8313	0.8268
F _{zero} (%)	14.29	13.79	12.90	17.74	19.67	16.95	17.74	16.00
F _{ab} (%)	33.97	33.12	35.43	35.38	36.68	37.34	37.14	37.19

Table 2 Prediction performance on one-hour wind speed dataset using the proposed method

	pos_1	pos_2	pos_3	pos_4	pos_5	pos_6	pos_7	pos_8
RMSE	0.6035	0.7022	0.7835	0.8102	0.8375	0.8751	0.8772	0.8878
F _{zero} (%)	44.92	38.85	36.59	36.23	34.53	32.00	45.33	48.32
F _{ab} (%)	59.85	60.45	62.76	62.26	62.96	62.96	61.36	60.65

Table 3 Prediction performance on one-day wind speed dataset using the proposed method

	pos_1	pos_2	pos_3	pos_4	pos_5	pos_6	pos_7	pos_8
RMSE	13.0654	14.0184	16.8574	17.8972	16.8697	18.8935	19.8352	20.2148
F _{ab} (%)	49.32	51.18	51.44	50.93	51.79	53.05	52.09	53.15

Table 4 Prediction performance on one-day wind speed dataset using LSTM model

	pos_1	pos_2	pos_3	pos_4	pos_5	pos_6	pos_7	pos_8
RMSE	5.9319	6.3825	6.7907	6.9861	7.0275	7.2854	7.5753	7.6748
F _{ab} (%)	67.41	70.73	71.03	72.24	73.70	73.05	73.80	73.40

Table 5 Prediction performance on one-hour non-zero wind speed dataset using the proposed method

	pos_1	pos_2	pos_3	pos_4	pos_5	pos_6	pos_7	pos_8
RMSE	0.8898	1.0917	1.2199	1.2510	1.2580	1.2908	1.3311	1.3355
F _{ab} (%)	58.39	60.10	63.37	62.81	63.77	63.67	62.11	61.16

The LSTM model is also employed for one-day wind speed prediction, serving as a benchmark against the proposed method. As delineated in Table 4, the *RMSE* values obtained across the eight positions consistently remain below 7.6748, underscoring superior performance compared to the proposed methodology. These findings suggest that the LSTM model possesses a distinct advantage in forecasting short-term wind speeds. Additionally, the $F_{\rm ab}$ achieved by the LSTM model exceeds 67.41%, significantly surpassing the values attained by the proposed method. These results provide compelling evidence of LSTM's efficacy in predicting short-term abnormal wind speeds.

3.5 The proposed method applied to one-hour non-zero wind speed prediction

The pre-processing of the non-zero wind speed time series involves applying EEMD and phase space reconstruction methods, followed by prediction using an LSTM network. Analysis of the results presented in Table 5 reveals that the proposed methodology yields higher RMSE values across the eight positions when applied to the non-zero wind speed dataset compared to its performance on the one-hour wind speed dataset. Moreover, the $F_{\rm ab}$ metric achieved on the non-zero wind speed dataset. These findings collectively suggest that the proposed method demonstrates superior performance in predicting abnormal wind speeds within non-zero wind speed data.

Table 6 Comparison of average performance at eight anemometers

Algorithm	Data	RMSE	F _{ab} (%)	F _{zero} (%)
LSTM	One-hour	0.7614	35.78	16.14
	One-day	6.9567	71.92	-
Proposed	One-hour	0.7971	61.66	39.60
	Non-zero	1.2092	61.92	-
	One-day	17.2064	51.62	-

3.6 The comparison of prediction performance on wind speed time-series datasets

Table 6 presents a comparative performance analysis of the LSTM model and the proposed methodology. Notably, the LSTM model achieves the lowest *RMSE* of 0.7614 on the one-hour wind speed dataset.

In evaluating prediction performance, the F_{-} Score metric is employed, where higher scores denote superior performance. For abnormal wind speed prediction, as shown in Fig. 2, LSTM attains a F_{ab} score of 35.78% on the one-hour wind speed dataset. This is surpassed by the proposed method, which yields F_{ab} scores of 61.66% and 61.92% on the one-hour and non-zero wind speed datasets, respectively. These results suggest that incorporating non-zero data marginally enhances abnormal wind speed prediction performance and underscores the proposed method's advantage in ultra-short-term abnormal wind speed predictions. However, on the one-day wind speed dataset, the proposed method achieves a lower F_{ab} score of 51.62% compared to LSTM's score of 71.92%. This

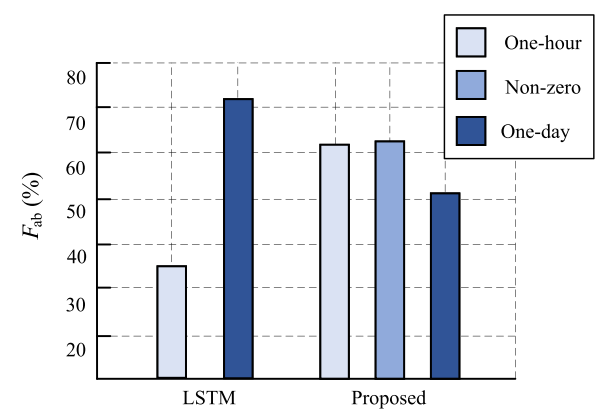


Fig. 2 The prediction performance of LSTM and the proposed method evaluated by $F_{\rm ah}$ (%)

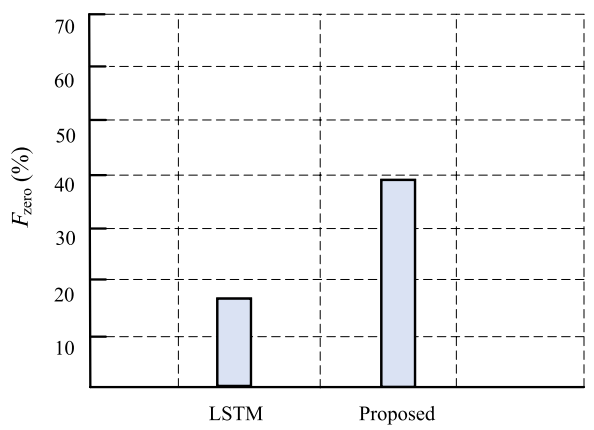


Fig. 3 The prediction performance of LSTM and the proposed method evaluated by F_{ZPTO} (%)

discrepancy highlights LSTM's advantage in short-term abnormal wind speed prediction. The superior performance of LSTM in short-term prediction may be attributed to the reduced noise in short-term wind speed data.

In the context of zero wind speed prediction, as shown in Fig. 3, the proposed methodology yields $F_{\rm zero}$ metric of 39.60% on the one-hour wind speed dataset, outperforming the LSTM model, which achieves a $F_{\rm zero}$ of 16.14% on the same dataset. This outcome underscores the efficacy of the proposed method in enhancing prediction performance for zero wind speed scenarios.

4 Conclusions

This study introduces a novel approach that integrates EEMD, phase space reconstruction, and LSTM networks for predicting abnormal wind speeds. We evaluate the method using three distinct wind speed datasets: one-hour wind speed, non-zero wind speed, and one-day wind speed scenarios. The comparative analysis of

experimental results demonstrates the effectiveness of our proposed methodology in significantly enhancing the prediction accuracy of ultra-short-term abnormal wind speeds. Furthermore, these experiments confirm the superior performance of the LSTM model in short-term abnormal wind speed prediction. However, it is noteworthy that both the proposed method and the LSTM model achieve $F_{\rm S}$ core values below 71.92% in abnormal wind speed prediction, and the $F_{\rm S}$ core for zero wind speed prediction by the proposed method remains below 39.60%. Future work will focus on integrating wind pressure and direction as input variables, potentially through a multivariate prediction model and refining the model architecture.

Acknowledgements

This work was supported in part by the National Natural Science Foundation of China (Grant No. 61971388).

Additional information

Edited by: Lin Gao.

Authors' contributions

Conceptualization, Yuting Yang and Yu Xue; methodology, Yuting Yang; software, Yuting Yang; validation, Kin-Man Lam, Yu Xue and Xin Sun; formal analysis, Xin Sun; investigation, Yu Xue; resources, Yuting Yang; data creation, Yuting Yang; writing-original draft preparation, Yuting Yang; writing-review and editing, Cong Zhang and Kin-Man Lam; visualization, Cong Zhang and Yu Xue; supervision, Kin-Man Lam; project administration, Yu Xue; funding acquisition, Xin Sun. All authors have read and agreed to the published version of the manuscript.

Data availability

The data used in this study is available from the fifth author on reasonable request.

Declarations

Ethics approval and consent to participate

Not applicable

Consent for publication

Not applicable.

Competing interests

The authors declare no conflicts of interest.

Received: 7 December 2024 Revised: 21 December 2024 Accepted: 20 January 2025

Published online: 27 February 2025

References

Bórawski P, Bełdycka-Bórawska A, Jankowski KJ, Dubis B, Dunn JW (2020) Development of wind energy market in the European Union. Renew Energy 161:691–700

Chang JC, Yang AM, Gong DX, Wang Z (2009) Analysis of 2D intrinsic mode function. In: 2009 International Conference on Test and Measurement, Hong Kong, pp 307–310

Che Y, Peng X, Delle Monache L, Kawaguchi T, Xiao F (2016) A wind power forecasting system based on the weather research and forecasting model and Kalman filtering over a wind-farm in Japan. J Renew Sustain Energy 8(1):013302

- Choi JH, Ahn SJ, Park JW, Moon SI (2009) Active power limitation of wind farm to reduce system operating cost. In: Transmission and Distribution Conference and Exposition-Asia and Pacific, Seoul, pp 1–4
- Chi P, Zhang Z, Liang R, Hu Y, Ni K, Li W (2022) A fault diagnosis method of double-layer LSTM for 10 kV single-core cable based on multiple observable electrical quantities. Electr Eng 104(2):603–614
- Demirtop A, Sevli O (2024) Wind speed prediction using LSTM and ARIMA time series analysis models: a case study of Gelibolu. Turk J Eng 8:524–536
- Fourure D, Javaid MU, Posocco N, Tihon S (2021) Anomaly detection: how to artificially increase your F1-Score with a biased evaluation protocol. Preprint at arXiv:2106.16020
- García-Marín AP, Estévez J, Jiménez-Hornero FJ, Ayuso-Muñoz JL (2013) Multifractal analysis of validated wind speed time series. Chaos-Int J Nonl Sci 23(1):97–106
- Hochreiter S, Schmidhuber J (1997) Long short-term memory. Neural Comput 9(8):1735–1780
- Kamath PR, Senapati K (2021) Short-term wind speed forecasting using S-transform with compactly supported kernel. Wind Energy 24(3):260–274
- Kennel MB, Brown R, Abarbanel HD (1992) Determining embedding dimension for phase-space reconstruction using a geometrical construction. Phys Rev A 45(6):3403
- Lange M, Focken U (2006) Physical approach to short-term wind power prediction. Springer Berlin, Heidelberg
- Lei Z, Sun X, Xing B, Hu Y, Jin G (2018) Active disturbance rejection based MPPT control for wind energy conversion system under uncertain wind velocity changes. J Renewa Sustain Energy 10(5):053307
- Leme Beu CM, Landulfo E (2024) Machine-learning-based estimate of the wind speed over complex terrain using the long short-term memory (LSTM) recurrent neural network. Wind Energy Sci 9:1431–1450
- Li GQ, Yang N (2023) A hybrid SARIMA-LSTM model for air temperature fore-casting. Adv Theory Simul 6(2):2200502
- Li L, Liu YQ, Yang YP, Shuang H, Wang YM (2013) A physical approach of the short-term wind power prediction based on CFD pre-calculated flow fields. J Hydrodyn 25(1):56–61
- Lin ZF, Cheng LL, Huang GH (2020) Electricity consumption prediction based on LSTM with attention mechanism. IEEJ Trans Electr Electron Eng 15(4):556–562
- Liu Y, Wang Y, Li L, Han S, Infield D (2016) Numerical weather prediction wind correction methods and its impact on computational fluid dynamics based wind power forecasting. J Renew Sustain Energy 8(3):033302
- Mohapatra MR, Radhakrishnan R, Shukla RM (2023) A hybrid approach using ARIMA, Kalman filter and LSTM for accurate wind speed forecasting. In: 2023 IEEE International Symposium on Smart Electronic Systems (iSES), Ahmedabad, pp 425–428
- Nelson V (2009) Wind energy: renewable energy and the environment. CRC Press, Boca Raton
- Neshat M, Nezhad MM, Abbasnejad E, Tjernberg LB, Garcia DA, Alexander B et al (2020) An evolutionary deep learning method for short-term wind speed prediction: a case study of the lillgrund offshore wind farm. Preprint at arXiv:2002.09106
- Packard NH, Crutchfield JP, Shaw RS (2008) Geometry from a time series. Phys Rev Lett 45:712
- Pont O, Turiel A, Yahia H (2013) Singularity analysis of digital signals through the evaluation of their unpredictable point manifold. Int J Comput Math 90(8):1693–1707
- Shahid F, Zameer A, Iqbal MJ (2021) Intelligent forecast engine for short-term wind speed prediction based on stacked long short-term memory. Neural Comput Appl 33(20):13767–13783
- Shi KL, Steigleder T, Schellenberger S, Schellenberger S, Michler F, Malessa A et al (2021) Contactless analysis of heart rate variability during cold pressor test using radar interferometry and bidirectional LSTM networks. Sci Rep 11(1):1–13
- Suman KM, Hussein Y (2019) A feature based reconstruction model for fluorescence microscopy image denoising. Sci Rep 9(1):7725
- Tao C, Lu J, Lang J, Peng X, Cheng K, Duan S (2021) Short-term forecasting of photovoltaic power generation based on feature selection and bias compensation-LSTM network. Energies 14(11):3086
- Wallot S, Mønster D (2018) Calculation of average mutual information (AMI) and false-nearest neighbors (FNN) for the estimation of embedding

- parameters of multidimensional time series in matlab. Front Psychol 9:1679
- Wang J, Yang ZS (2021) Ultra-short-term wind speed forecasting using an optimized artificial intelligence algorithm. Renew Energy 171(5):1418–1435
- Wu ZH, Huang NE (2004) A study of the characteristics of white noise using the empirical mode decomposition method. Proc R Soc London Ser A 460(2046):1597–1611
- Wu ZH, Huang NE (2009) Ensemble empirical mode decomposition: a noiseassisted data analysis method. Adv Ada Data Anal 1(1):1–41

Publisher's Note

Springer Nature remains neutral with regard to jurisdictional claims in published maps and institutional affiliations.